ESR AND MICROWAVE CONDUCTIVITY STUDIES IN DEM$(TCNQ)_2$ ABOVE ROOM TEMPERATURE

by

FRANCISCO XAVIER CABAÑAS

B.Sc. The University of British Columbia, 1979

A THESIS SUBMITTED IN PARTIAL FULFILMENT OF
THE REQUIREMENTS FOR THE DEGREE OF
MASTER OF SCIENCE

in

THE FACULTY OF GRADUATE STUDIES
(Department of Physics)

We accept this thesis as conforming
to the required standard

THE UNIVERSITY OF BRITISH COLUMBIA
November 1981

In presenting this thesis in partial fulfilment of the requirements for an advanced degree at the University of British Columbia, I agree that the Library shall make it freely available for reference and study. I further agree that permission for extensive copying of this thesis for scholarly purposes may be granted by the head of my department or by his or her representatives. It is understood that copying or publication of this thesis for financial gain shall not be allowed without my written permission.

Department of Physics

The University of British Columbia
2075 Wesbrook Place
Vancouver, Canada
V6T 1W5

Date 24th Nov 1981

ABSTRACT

Two phase transitions have been found in $DEM(TCNQ)_2$ at 400(3) K and at 442(6) K to 453(6) K using ESR and measurements of the microwave conductivity. These temperatures are less than the values of 415 K and 483 K previously obtained from temperature dependent Guinier measurements. Below 400(3) K two ESR lines, I and II are observed corresponding to the two stacks, B and A, in $DEM(TCNQ)_2$. Above 400(3) K and below 453(6) K only one line remains with the same g value as line I. The angular dependence of the g value was fitted to $g^2 = g_{\parallel}^2\cos^2\theta + g_{\perp}^2\sin\theta$ and values of $g_{\perp} = 2.003551(14)$ and $g_{\parallel} = 2.002730(15)$ were obtained. Between 298 K and 442(6) K the conductivity was that of a semiconductor with an exitation energy $E_o = 0.385(52)$ e.v. The $4k_F$ phase transition is postulated at 447(9) K. The phase transition at 400(3) K is due to a transfer of spin density from stack A to stack B, and has no effect on the total spin susceptibility or on the conductivity to within the experimental error.

TABLE OF CONTENTS

LIST OF TABLES

LIST OF FIGURES

ACKNOWLEGEMENTS

I wish to express my gratitude to my supervisor, Dr. C. F. Schwerdtfeger, for his supervision, assistance, and exchange of ideas both during the performance of the experiments and the preparation of the thesis.

I would also like to thank Dr. J. F. Carolan who read the thesis for his suggestions and comments.

I am also indebted to Dr. G. A. Sawatzky and Dr. B. van Bodegom of the University of Groningen for providing the $DEM(TCNQ)_2$ samples.

A post graduate scholarship from the Natural Sciences and Engineering Research Council of Canada is gratefully acknowleged. Research for this thesis was funded by the Natural Sciences and Engineering Research Council of Canada through grants to Dr. Schwerdtfeger.

CHAPTER 1 INTRODUCTION

1.1 SIGNIFICANCE OF DEM(TCNQ)$_2$ AND RELATED COMPOUNDS

N–ethyl–N–ethyl–morpholinium tetracyanoquidimethane, DEM(TCNQ)$_2$, is a member of a family of related compounds where the morpholinium group changes. When the radical denoted by R in figure 1.1 is replaced by C_2H_5 we have DEM(TCNQ)$_2$, by CH_3 we have MEM(TCNQ)$_2$ (MEM = N–methyl–N–ethyl–morpholinium), and by H we have HEM(TCNQ)$_2$ (HEM = N–ethyl–morpholinium). The significant characteristic of these compounds is the quasi one–dimensional behaviour of the electrical conductivity. This provides an example of a physical system where one–dimensional theory can be tested. The Hubbard Hamiltonian

$$H = -\sum_{i,\sigma} t_{i,i+1} \left(c^{+}_{i,\sigma} c_{i+1,\sigma} + c^{+}_{i+1,\sigma} c_{i,\sigma}\right) + \sum_{i} U n_{i,\sigma} n_{i,-\sigma} \qquad (1.1)$$

and the prediction of $2k_F$ and $4k_F$ instabilities depending on the value of U/t has been crucial to this theory (see Huizinga 1980 p.2)

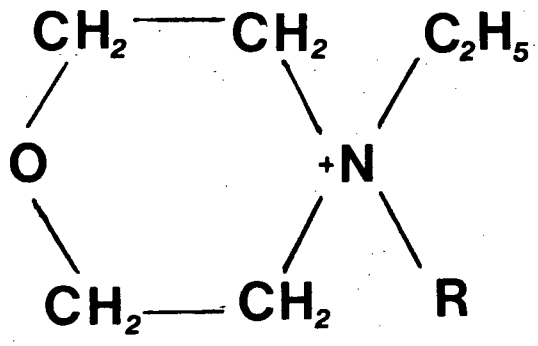

Figure 1.1 The MEM, DEM and HEM Molecules R = CH_3 : MEM ; R = C_2H_5 : DEM ; R = H : HEM

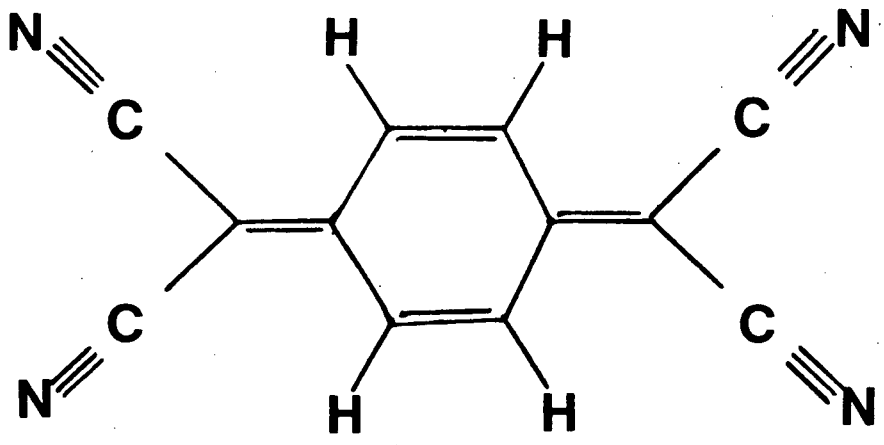

Figure 1.2 The TCNQ Molecule

Measurements have been performed on $MEM(TCNQ)_2$ and $HEM(TCNQ)_2$. The crystal structure of $MEM(TCNQ)_2$ at 113 K has been reported by Bosh and van Bodegom (1977). Two phase transitions have been found in $MEM(TCNQ)_2$ at 18 K and 340 K.

The specific heat of $MEM(TCNQ)_2$ has been reported by Sawatzky et al. (1980). They report a peak in the specific heat at 19 K with an entropy gain of 1.4J–mole/K, and another peak at 335 K with an entropy gain of 14J–mole/K, corresponding to the two phase transitions in $MEM(TCNQ)_2$.

Huizinga, Kommandeur, Sawatzky, and Thole report a Spin–Peierls phase transition at 18 K. The high temperature conductivity of $MEM(TCNQ)_2$ has been measured by Morrow et al. (1980), where a reversible semiconductor–metal phase transition is reported at 340 K. Huizinga (1980) has correlated the phase transitions at 18 K and 340 K in $MEM(TCNQ)_2$ with the $2k_F$ and $4k_F$ instabilities.

The crystal structure of the related compound $HEM(TCNQ)_2$ has been measured by van Bodegom and van de Boer (1981). A phase transition at 450 K using a Differential Scanning Calorimeter (DSC) technique and a sharp decline in the spin susceptibility at 425 K, indicating a phase transition, has been reported by Huizinga (1980 p.108) in $HEM(TCNQ)_2$. This phase transition is attributed by Huizinga to be related to the $2k_F$ instability predicted from the theory, implying that U/t_o is much less for $HEM(TCNQ)_2$ than for $MEM(TCNQ)_2$ (see Huizinga 1980 p.101).

1.2 CHARACTERISTICS OF DEM(TCNQ)$_2$

The crystal structure of DEM(TCNQ)$_2$ has been measured by Morrsink and van Bodegom (1981). They report two types of TCNQ sheets, A and B, that are at an angle of 60° (see fig.1.3). This makes DEM(TCNQ)$_2$ fundamentally different from MEM(TCNQ)$_2$ or HEM(TCNQ)$_2$.

Sheet B behaves in a one-dimensional fashion and is similar to MEM(TCNQ)$_2$ in its behavior below room temperature. A Spin-Peierls phase transition has been observed in sheet B of DEM(TCNQ)$_2$ at 23 K by Schwerdtfeger, Oostra and Sawatzky. This compares to the Spin-Peierls phase transition at 18 K in MEM(TCNQ)$_2$. This phase transition probably corresponds to the $2k_F$ instability in the stack of TCNQ molecules in sheet B of DEM(TCNQ)$_2$.

Unlike the stacks in sheet B, the stacks in sheet A do not undergo a Spin-Peierls phase transition between 1.5 K and room temperature. The latter stack remains paramagnetic down to 1.5 K. While stack B has been shown to behave in a similar manner to the single stack of TCNQ molecules in MEM(TCNQ)$_2$; the corresponding stack for sheet A behaves more like a two-dimensional system (Schwerdtfeger, Oostra and Sawatzky).

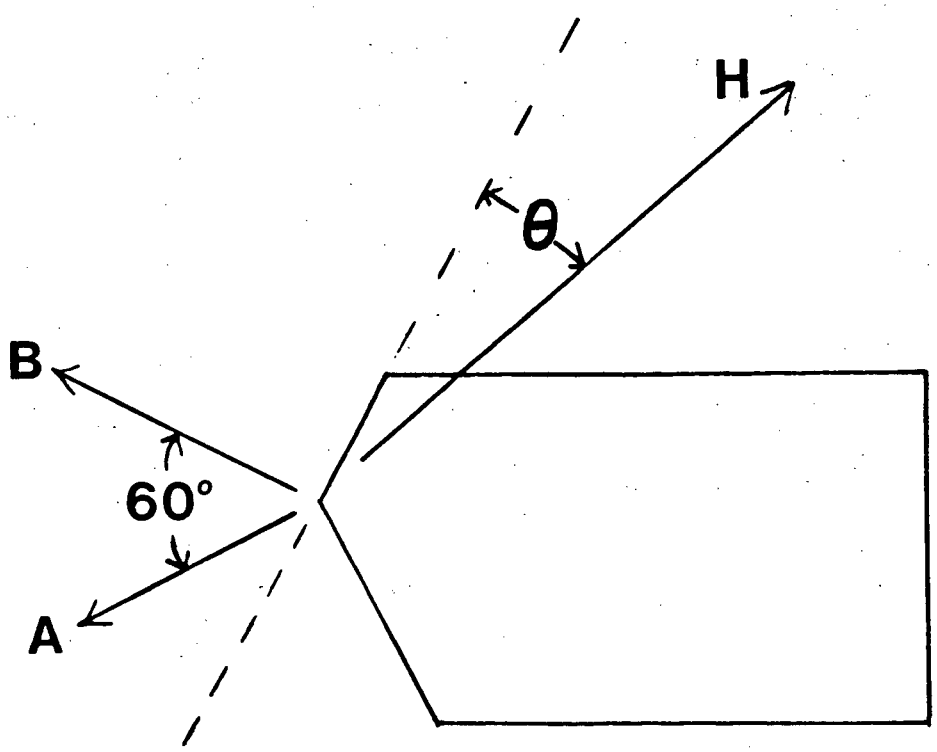

Figure 1.3 Shape of a Typical DEM(TCNQ)$_2$ Crystal. The Arrows Labelled A and B Indicate the Directions of Stacks A and B Respectively and the Arrow Labelled H Indicates the Direction of the Static Magnetic Field for the ESR Measurements.

At high temperatures Morrsink and van Bodegom report two reversible phase transitions at 415 K and 483 K in $DEM(TCNQ)_2$. The ESR spectra of $DEM(TCNQ)_2$ between 23 K and 298 K has two lines I and II that originate in sheets B and A respectively. We follow the notation of Schwerdtfeger, Wagner and Sawatzky (1980). The angular dependence of the values of g at 77 K and 198 K, and of g at 1.14 K, 4.2 K, 77 K, and 298 K are reported by Schwerdtfeger Wagner and Sawatzky (1980) (see table 5.2). The spin-susceptibility and halfwidth of lines I and II as a function of temperature has been measured by Schwerdtfeger, Oostra and Sawatzky.

A qualitative similarity between the bulk susceptibilities of $DEM(TCNQ)_2$ and $MEM(TCNQ)_2$ in the temperature range from 4 K to 300 K is reported by Kuindersma, Sawatzky and Kommandeur (1975). There are indications that the contribution to the bulk susceptibility from stacks A and B are similar, however there is a fundamental difference in the nature of the stacks A and B in $DEM(TCNQ)_2$.

1.3 OUTLINE

In chapter 2 we present the theory behind the microwave conductivity measurements and a description of the apparatus and experimental procedure used to measure the microwave conductivity.

The microwave conductivity data as a function of

temperature between 290 K and 480 K, showing a phase transition at 442(6) K together with the real part of the dielectric constant at room temperature is presented in chapter 3.

In chapter 4 we present a description of the ESR apparatus and the experimental procedure, together with the numerical methods used in the analysis of the ESR data.

Chapter 5 contains the ESR results. These results include: The spin susceptibilities of lines I and II, the sum of the spin susceptibilities of lines I and II, and the peak to peak halfwidth of lines I and II as a function of temperature, the phase transition temperatures that were found at 400(3) K and 453(6) K in the susceptibility and halfwidth data, the angular dependence of the g value and halfwidth, measured at T=400(3) K, of the only line above the phase transition at 400(3) K, and the g values, measured at $\theta = 60°$ (see fig. 1.3), of both line below the phase transition at 400(3) K and the single line above 400(3) K.

Chapter 6 contains a comparison between the results for $DEM(TCNQ)_2$ and the results for $MEM(TCNQ)_2$ and $HEM(TCNQ)_2$ together with a correlation of the different phase transition temperatures in $DEM(TCNQ)_2$ with the two postulated phase transitions in $DEM(TCNQ)_2$ above room temperature.

General conclusions and some further experiments on $DEM(TCNQ)_2$ are presented in chapter 7.

CHAPTER 2 DIELECTRIC CONSTANT AND CONDUCTIVITY THEORY AND MEASUREMENTS

2.1 THEORY OF CAVITY PERTURBATION

If a dielectric sample of volume V_1 is introduced into a resonant cavity of volume V_0 the shift in the complex frequency for small perturbations is

$$\frac{\Omega_0-\Omega_1}{\Omega_0} = \frac{-\int_{V_1}[(\underline{E}_1\cdot\underline{D}_0-\underline{E}_0\cdot\underline{D}_1)-(\underline{H}_1\cdot\underline{B}_0-\underline{H}_0\cdot\underline{B}_1)]dV}{\int_{V_0}[\underline{E}_0\cdot\underline{D}_0-\underline{H}_0\cdot\underline{B}_0]dV} \qquad (2.1)$$

where $\Omega_0 = 2\pi\nu_0(1+i/2Q_0)$ and $\Omega_1 = 2\pi\nu_1(1+i/2Q_1)$ are the unperturbed and perturbed complex frequencies respectively (Waldron,1969.pp.87-93). In the experiments the frequency of the cavity with the sample holder alone, Ω_H, and the frequency of the cavity with the sample holder and the sample, Ω_S, were measured. If we assume that the field displaced by the sample is the unperturbed field, and approximating Ω_0 by Ω_H in the denominator of (2.1) we obtain

$$\frac{\Omega_H - \Omega_S}{\Omega_H} = \frac{-\int_{V_1}[(\underline{E}_S\cdot\underline{D}_0-\underline{E}_0\cdot\underline{D}_S)-(\underline{H}_S\cdot\underline{B}_0-\underline{H}_0\cdot\underline{B}_S)]dV}{\int_{V_0}[\underline{E}_0\cdot\underline{D}_0-\underline{H}_0\cdot\underline{B}_0]dV} \qquad (2.2)$$

where $\underline{E}_0+\underline{E}_S$, $\underline{D}_0+\underline{D}_S$, $\underline{H}_0+\underline{H}_S$, and $\underline{B}_0+\underline{B}_S$, are the electric and magnetic fields in the sample, and V_S is the volume of the sample. For non magnetic samples $\underline{H}_0=\underline{B}_0=\underline{0}$. If the sample is ellipsoidal, the dimensions of the sample are much less than a wavelength, and the skindepth is larger than or close to the smallest dimension of the sample, then the field in the sample is

$$\underline{E}_0+\underline{E}_S = \frac{\underline{E}_0}{1+n(\hat{\epsilon}-1)} \qquad (2.3)$$

where n is the depolarizing factor and $\hat{\epsilon}=\epsilon'+i\epsilon''$ is the complex dielectric constant of the sample (Buranov et al,1971,p.528). If equation (2.3) is substituted into equation (2.2), then equating real and imaginary parts and assuming that $\underline{E}_0$ is constant over the volume of the sample, we obtain for a sample on the axis of a cylindrical cavity

$$\frac{1}{2}\left(\frac{1}{Q}-\frac{1}{Q}\right) = \frac{a\epsilon''}{\{[1+n(\epsilon'-1)]^2+(n\epsilon'')^2\}} \qquad (2.4)$$

and

$$\frac{\nu_S-\nu_H}{\nu_H} = \frac{a\{(\epsilon'-1)[1+n(\epsilon'-1)+n(\epsilon'')^2]\}}{\{1+n(\epsilon'-1)\}^2+(n\epsilon'')^2} \qquad (2.5)$$

where

$$\alpha = \frac{V_S \epsilon_0 E_{0MAX}^2}{\int_{V_0} \{\underline{E}_0 \cdot \underline{D}_0 - \underline{H}_0 \cdot \underline{B}_0\} dV} \qquad (2.6)$$

E_{0MAX} is the magnitude of the electric field on the axis of the cavity, and ϵ_0 is the permitivity of free space (Buranov et al,1971 p.528). For the TM_{010} mode

$$\int_{V_0} (\underline{E}_0 \cdot \underline{D}_0 - \underline{H}_0 \cdot \underline{B}_0) dV = \epsilon_0 E_{0MAX}^2 V_0 2J_1^2(ka) \qquad (2.7)$$

where $J_1(ka) = 0.51915$ (Waldron,1970 pp.303-305). α is then $1.8552V/V_0$. The solution of (2.4) and (2.5) for $\epsilon'-1$ and ϵ'' is

$$\epsilon'' = \frac{\alpha \Delta}{n^2 2}\left[\left(\frac{\Delta}{2}\right)^2 + \left(\frac{\alpha}{n} - \delta\right)^2\right]^{-1} \qquad (2.8)$$

and

$$\epsilon'-1 = \frac{1}{n}\left[\delta\left(\frac{\alpha}{n} - \delta\right) - \left(\frac{\Delta}{2}\right)^2\right] \Big/ \left[\left(\frac{\Delta}{2}\right)^2 + \left(\frac{\alpha}{n} - \delta\right)^2\right] \qquad (2.9)$$

where

$$\delta = \frac{\nu_S - \nu_H}{\nu_H} \quad \text{and} \quad \Delta = \frac{1}{Q_S} - \frac{1}{Q_H} \quad \text{(Buranov et al,1971 p.528)}$$

The quantities δ, Δ, N and α can be measured or calculated, and hence ϵ' and ϵ'' can be determined.

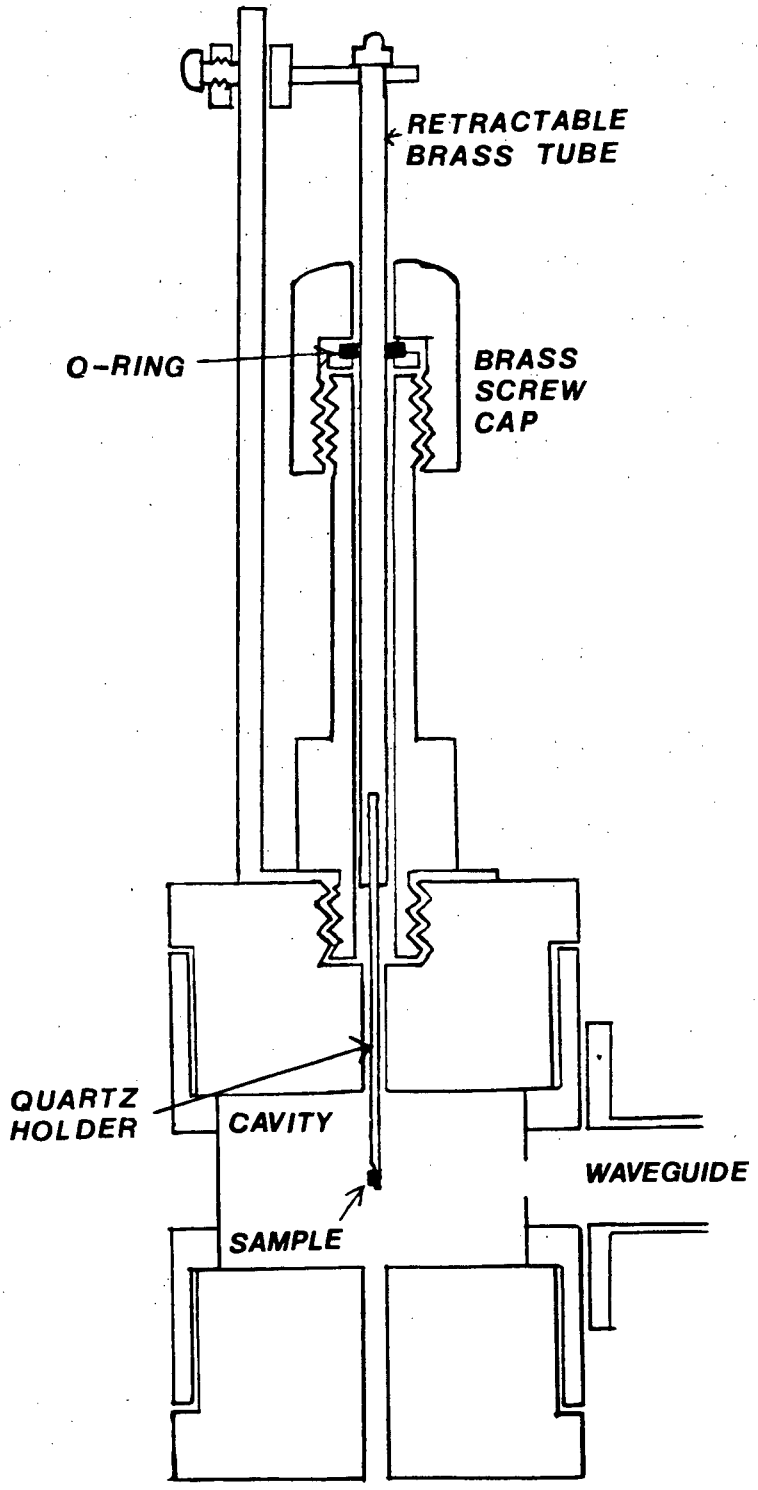

Figure 2.1 Cavity and Sample Holder used for Dielectric Constant and Conductivity Measurements.

2.2 DIELECTRIC CONSTANT MEASURING APPARATUS

The sample was mounted on the axis of a cylindrical cavity operating in the TM_{010} mode at 9.2 GHz (see fig. 2.1) the microwave source was an HP8620C sweep oscillator with an HP86250B RF plug in. The frequency was measured with an HP5245L frequency counter with an HP5255A frequency converter. Scans of the power reflected from the cavity as a function of frequency were obtained (see fig.2.2) from which the resonant frequency and the Q of the resonance were determined. A block diagram of the apparatus is shown in figure 2.3.

To obtain the coarse temperature the sample cavity was placed inside a glass cylinder that was wrapped with heating tape. The fine temperature was obtained by using two power resistors next to the cavity. The cavity and heating elements were then placed inside a glass dewer for insulation. Control of the fine temperature was accomplished by means of a resistance bridge using a thermistor as the temperature sensitive element. This provided a temperature stability of 0.1°C during each data scan.

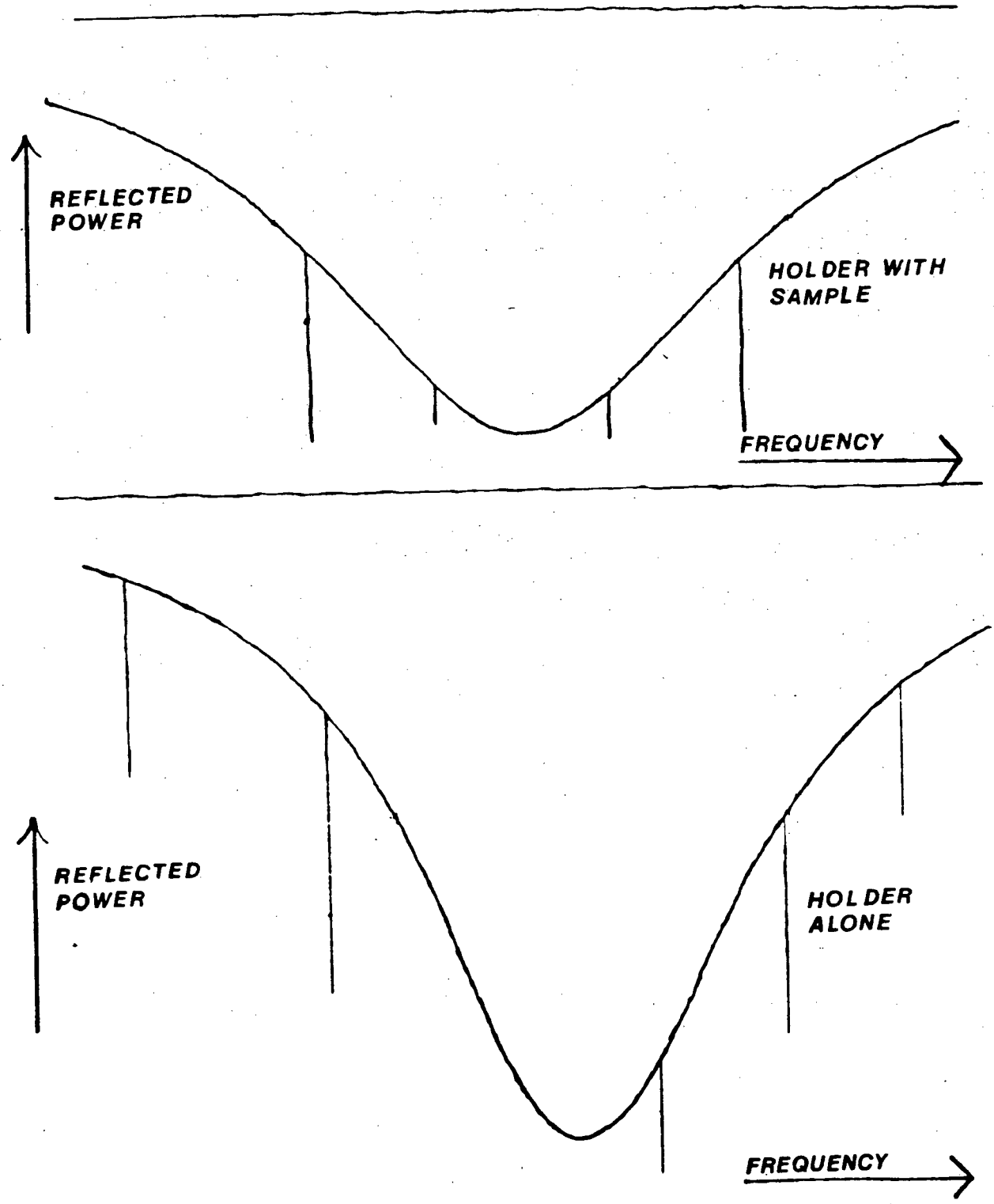

Figure 2.2 Resonance of the Cavity used for the Dielectric Constant and Conductivity Measurements with and without the Sample.

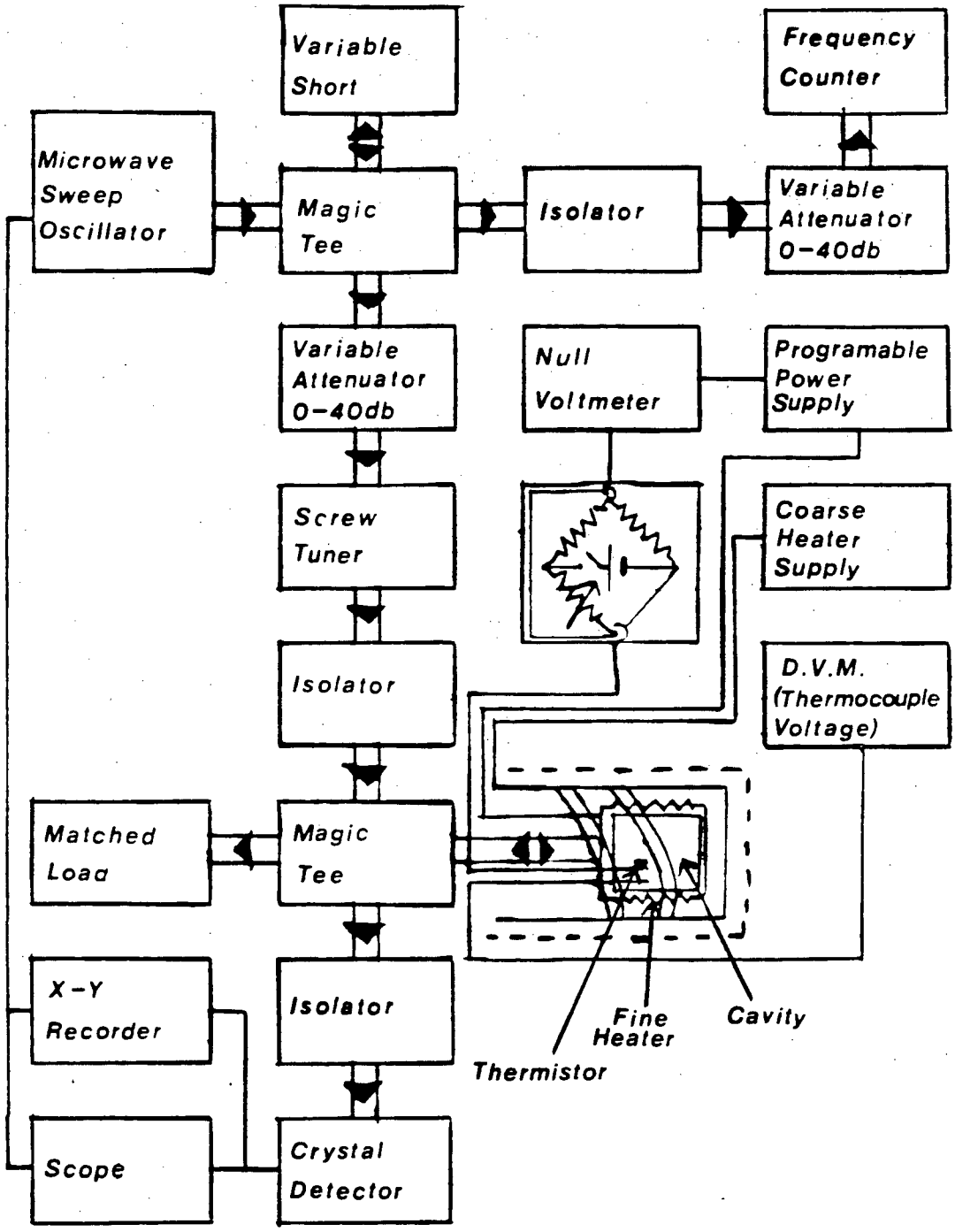

Figure 2.3 Block Diagram of the Dielectric Constant and Conductivity Apparatus.

2.3 DIELECTRIC CONSTANT AND CONDUCTIVITY MEASUREMENTS

The resonant frequencies of the cavity, perturbed by the sample holder, with and without the sample in place were measured as a function of temperature. In the latter case a least squares fit to the a straight line was made and the values of the resonant frequency and Q of the cavity were calculated for the temperatures corresponding to the scans where the cavity was perturbed by the sample holder and the sample. In this manner it was possible to determine at each temperature the resonant frequency and Q of the cavity owing to the empty sample holder.

In order to determine the depolarizing factor of the samples, the linear dimensions of the samples were measured on a travelling microscope and the depolarizing factors were obtained by interpolation from a plot of the Demagnetizing Factors of the General Ellipsoid (Osborn,1945 p.355). The approximation that the sample is ellipsoidal has to be made in order to apply equation (2.3). In making this approximation ellipsoids with the same volume and linear dimensional ratios as the samples were used.

The volumes of the samples were determined by weighing the samples and using the known density of $DEM(TCNQ)_2$, d_M= 1.253 mg mm^{-3}, (Morrsink et al, 1981 p.107). The volumes measured by this method agreed with the volumes obtained from the linear dimensions of the samples to within experimental error.

In equation (2.2) the electric field in the immediate

vicinity of the sample is assumed to be equal to the field in that location of the cavity without the sample. This assumption is valid because the volume of the sample as well as the volume of the sample holder are negligible when compared to the volume of the cavity.

TABLE 2.1 PHYSICAL DATA OF THE NYLON TEST SAMPLE

Sample	a(mm)	b(mm)	c(mm)	Volume (mm^3)	Depolarizing Factor
#1	4.66(2)	0.47(2)	0.33(2)	0.71(5)	0.015(3)

Another possible source of error is the shape of the sample holder. This was checked by measuring the dielectric constant and of nylon thread. A piece of nylon thread was measured and values of $\epsilon'=2.94$ and $\epsilon''=0.032$ were obtained (see table 2.1). This compares well with the published values of $\epsilon'=2.84-3.03$ and $\epsilon''=0.032-0.039$ (Von Hipple, pp.310–311,323).

CHAPTER 3 DIELECTRIC CONSTANT AND CONDUCTIVITY RESULTS

3.1 EXPERIMENTAL RESULTS

Three crystals of $DEM(TCNQ)_2$ were used in the dielectric constant and conductivity measurements. The physical data of the crystals are shown in table 3.1. The values a, b, and c are the principal axes of the approximating ellipsoid used in calculating the depolarizing factors. These values approximate the dimensions of the samples along the directions parallel and perpendicular to the electric field.

The microwave conductivity of the crystals as a function of temperature is plotted in fig 3.1 and in fig 3.2. The measured microwave conductivity was low enough so that the lowest value of the skin depth was greater than 1.8 mm. This is larger than the smallest dimension of the sample (see table 3.2). The room temperature dielectric constant and conductivity are summarized in table 3.2. It was only possible to obtain ϵ' at room temperature because the large depolarizing factor causes the measurements of ϵ' to be unreliable when the conductivity increases.

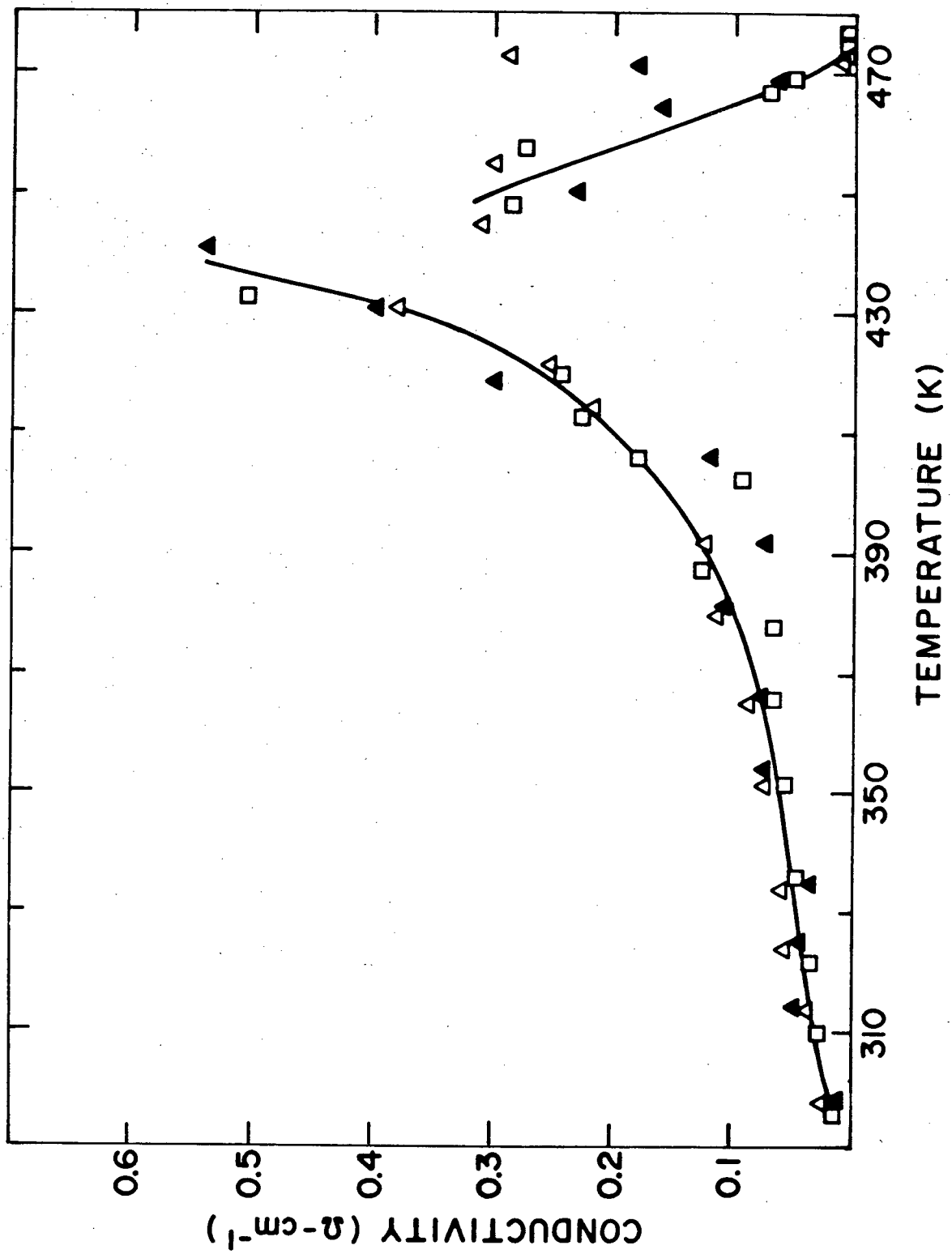

Figure 3.1 Microwave Conductivity of $DEM(TCNQ)_2$ vs Temperature △: Sample #1 □:Sample #2 ▲: Sample #3. The Solid Curve is Estimated from the Points.

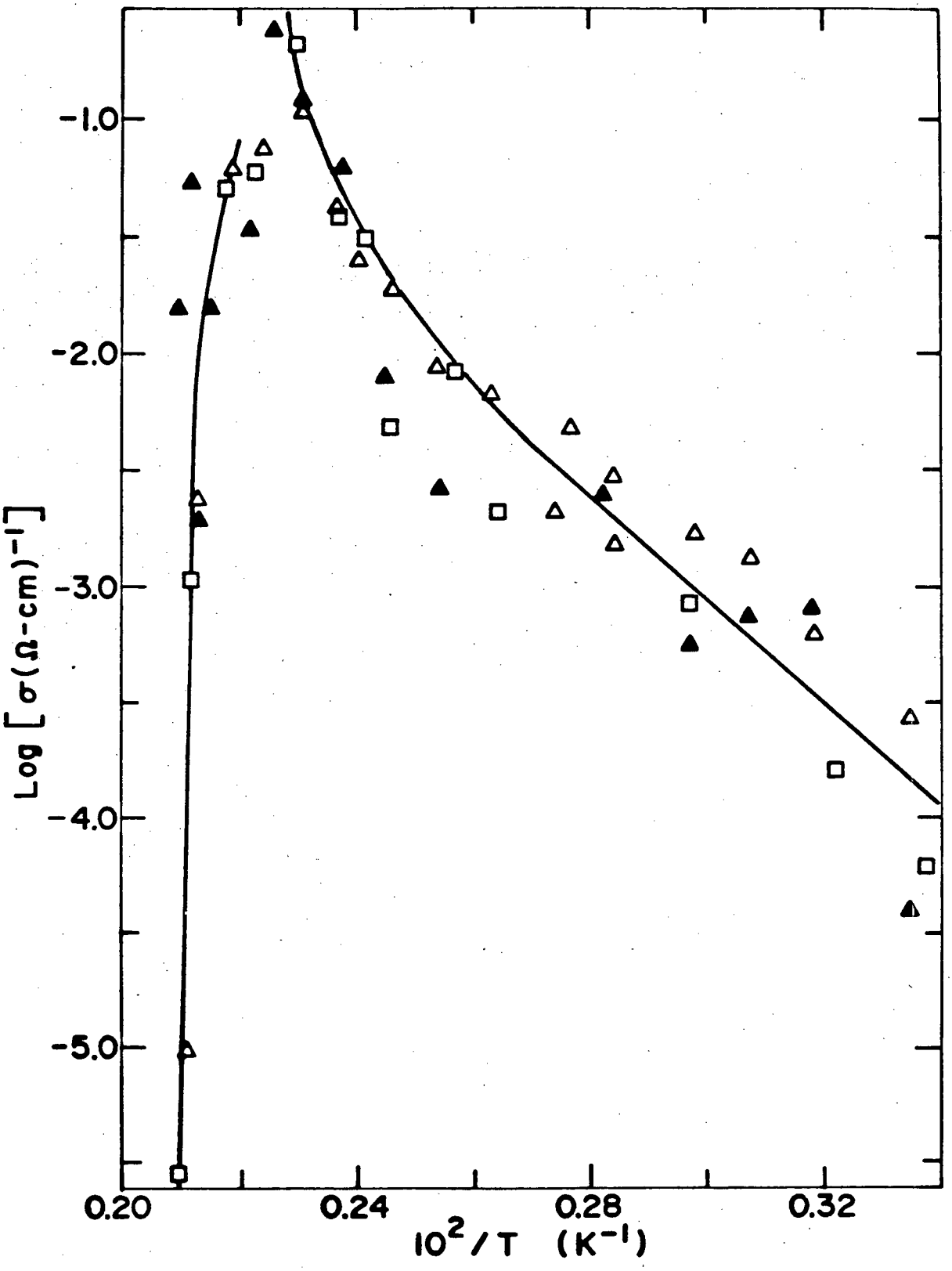

Figure 3.2 Natural Logarithm of the Microwave Conductivity of $DEM(TCNQ)_2$ vs Inverse Temperature. Symbols are defined in fig. 3.1. The Solid Curve is Estimated from the Points.

TABLE 3.1 PHYSICAL DATA OF $DEM(TCNQ)_2$ SAMPLES

Sample	a(mm)	b(mm)	c(mm)	Volume (mm^3)	Depolarizing Factor
#1	1.36(2)	0.62(2)	0.16(2)	0.1140(3)	0.055(5)
#2	0.92(2)	0.69(2)	0.15(2)	0.0651(3)	0.095(5)
#3	0.81(5)	0.75(5)	0.25(2)	0.1416(3)	0.165(15)

TABLE 3.2 EXPERIMENTAL RESULTS

Sample	ϵ' (Room-temp)	ϵ'' (Room-temp)	E_0 (e.v.)	$\ln\sigma_0$ $\ln\{(\Omega\text{-cm})^{-1}\}$
#1	11.0	5.5	0.328(26)	2.9(5)
#2	4.3	2.7	0.403(43)	3.8(7)
#3	11.6	2.4	0.43(12)	4.3(21)
average	9.0(23)	3.5(10)	0.389(52)	3.7(9)

The conductivity was found to follow a semiconductor like behavior below 370 K. The data was analysed in terms of the equation

$$\sigma = \sigma_0 \exp(-E_0/2kT) \qquad (3.1)$$

where E_0 is the band gap. The values of E_0 and $\ln\sigma_0$ obtained for the crystals are shown in table 3.2. Above 370 K deviations from an ordinary semiconductor behavior are observed and at a temperature of 442(6) K a discontinuity in the conductivity is observed, indicating a phase transition. Above the phase transition an abrupt decrease in the conductivity is observed. The heating of the sample was found to be non-reversible, owing to the fact that the samples lost 25% of their mass when they were heated between 450 K and 480 K, and the subsequent room temperature conductivity was sharply lower when the sample had been heated up to 480 K. This loss of mass together with the decrease of the conductivity indicates the decomposition of the sample above 450 K.

3.2 DISCUSSION OF THE DIELECTRIC CONSTANT AND CONDUCTIVITY MEASUREMENTS

(a) Quoted Experimental Errors

The errors in the dimensions of the samples were estimated using repeated measurements on a travelling microscope. The measurements for sample #3 have larger error because the sample's longest dimension was at an angle of about 30° to the electric field instead of along the electric field. This meant that estimates of the dimensions of the sample along the electric field and perpendicular to the electric field were used instead of the length, width, and thickness of the sample.

The quoted error in the depolarizing factor is due to the estimated errors in the dimensions of the samples. This error does not include any additional errors introduced by the approximation of the shape of the samples as ellipsoids.

The quoted errors for E_0 and $\ln\sigma_0$ for each sample are the standard errors from the fit of the conductivity data to

$$\ln\sigma = -E_0/2kT+\ln\sigma_0 \qquad (3.2)$$

where the parameters E_0 and $\ln\sigma_0$ are determined by the fit. This error incorporates the statistical error in the data for each sample, it does not incorporate any systematic errors. The values of E_0 and $\ln\sigma_0$ described as average in table 3.2 are determined from a fit to equation (3.2) using the data from the three samples. The errors in E_0 and $\ln\sigma_0$ obtained in this case

are the standard errors from the fit. These last errors will include some of the systematic error in as far as this error is systematic to one sample, but not systematic to all the measurements. The largest contribution to this kind of error comes from depolarizing factor. The errors quoted for ϵ' and ϵ'' for the average result are the standard error of the mean of the three measurements.

(b) Shape of the Samples as a Source of Error

The determination of ϵ' is limited by the depolarizing factor of the samples. A small depolarizing factor is desirable because it allows the electric field to penetrate inside the sample permitting a measurement of ϵ'. Another disadvantage of a large depolarizing factor is that the depolarizing factor is determined only approximately. If the terms that contain the depolarizing factor are dominant in equations (2.8) and (2.9) then the errors in the depolarizing factor together with the approximation of the sample shape by an ellipsoid would introduce significant errors into the final results.

The optimal shape to minimize the depolarizing factor is a very long and thin crystal where $a>>b>c$. The crystals used were selected for low depolarizing factor; however the available crystals were far from the optimal shape. This limited the accuracy of the experiment and precluded a measurement of ϵ' above room temperature.

CHAPTER 4 ESR APPARATUS, MEASUREMENTS AND SUSCEPTIBILITY CALCULATIONS

4.1 ESR APPARATUS

Electron spin resonance, ESR, was performed at X-band. The sample was placed in a rectangular cavity operating in the TE_{102} mode. The cavity was placed in a magnetic field that was swept through the ESR resonance. The magnetic field was modulated at 100 KHz by means of coils placed on the cavity exterior. The static field was measured by means of an NMR probe. The difference in field between the position of the NMR probe and the center of the cavity was calibrated with a standard ESR sample of LiF:Li, the NMR frequencies being measured on an HP5245L frequency counter.

The microwave source was a Varian VA-297 klystron operating at 9.2 GHz that was phase-locked to the sample cavity frequency. The microwave frequency was measured by an HP5245L frequency counter with an HP5255A frequency converter.

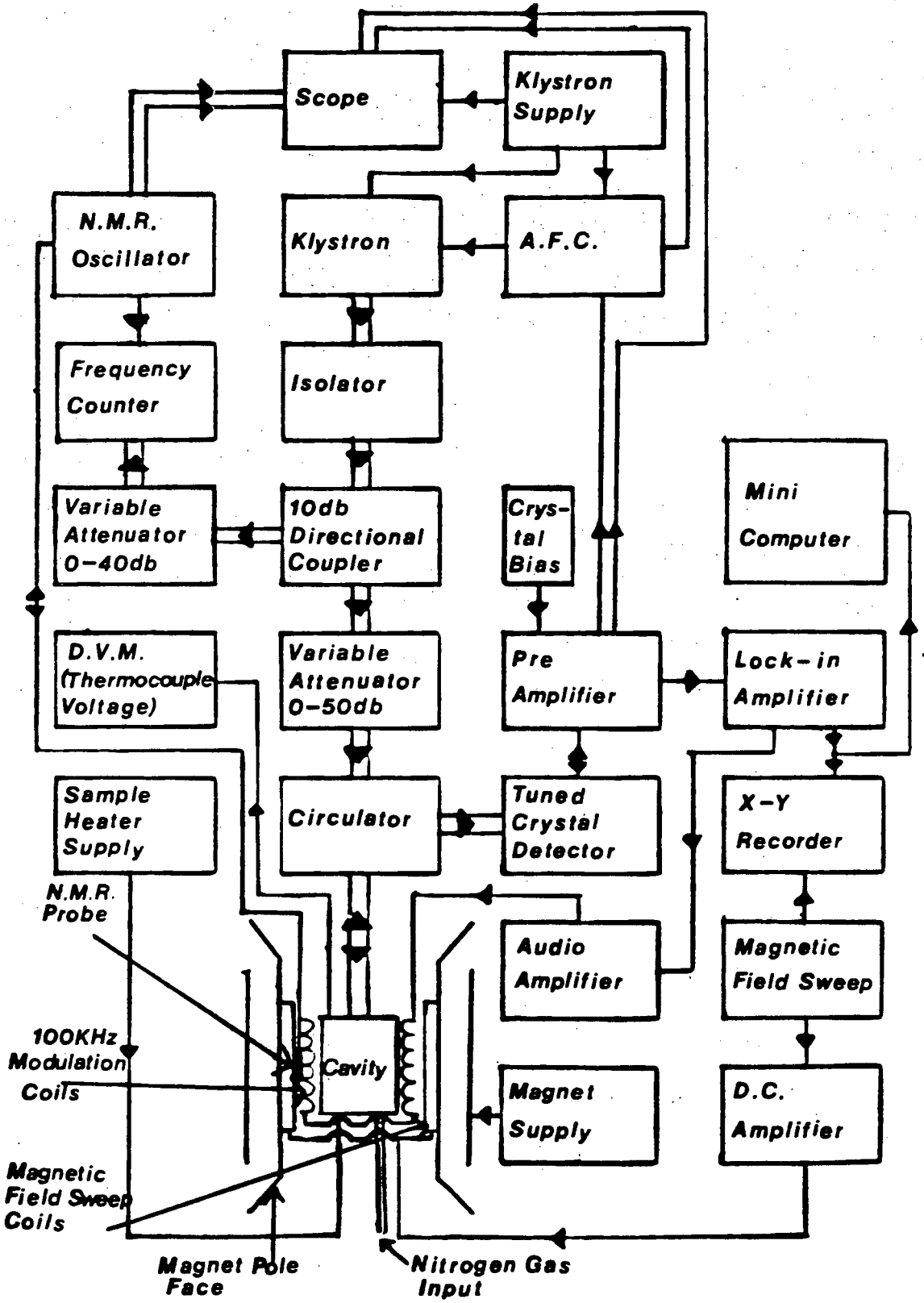

Figure 4.1 Block Diagram of the ESR Apparatus.

Absorption of the sample was detected with a lockin amplifier whose output gave the derivative of the ESR signal and after amplification was recorded on an X–Y recorder, or sampled digitally with a NOVA 2 microcomputer and punched out on paper tape. The digitized data could then be read into the UBC computing system for further processing. A block diagram of the apparatus is shown in fig. 4.1.

The sample was heated by means of a Varian flow system (fig. 4.2) using nitrogen gas as the heat transfer medium. The sample temperature was measured using an iron–constantan thermocouple with an ice bath as reference.

4.2 THE ESR MEASUREMENTS

Electron spin resonance (ESR) measurements were performed on $DEM(TCNQ)_2$ as a function of temperature between room temperature and 453(6) K. The g values of the two observed lines were measured as a function of temperature. Above the phase transition the g value of line I was measured as a function of the angle between the crystal axis and the magnetic field.

The spin susceptibilities and peak to peak widths were then determined by fitting the integral of the output derivative curve with convoluted Gaussian–Lorentzian functions.

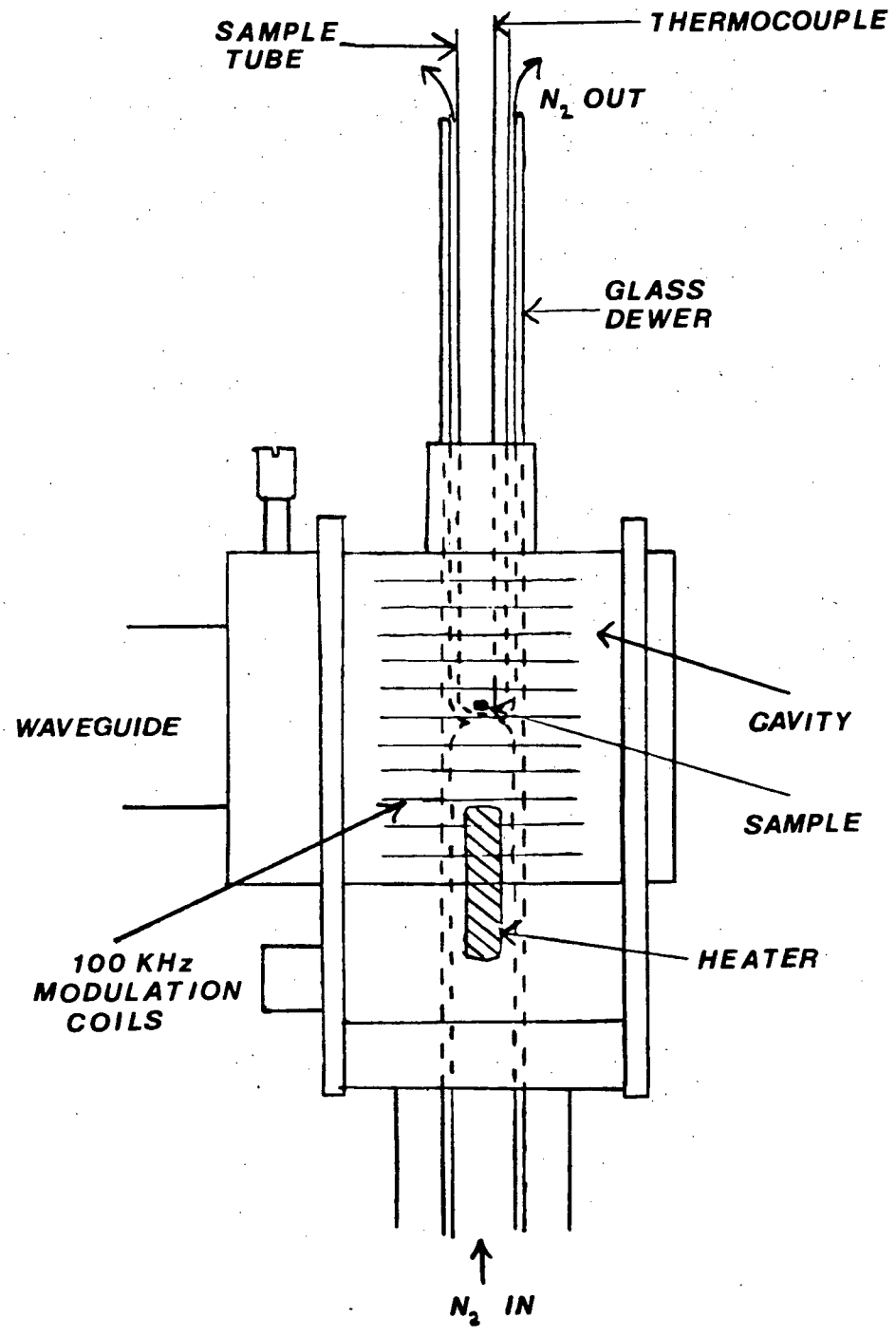

Figure 4.2 ESR Cavity and Varian Flow System.

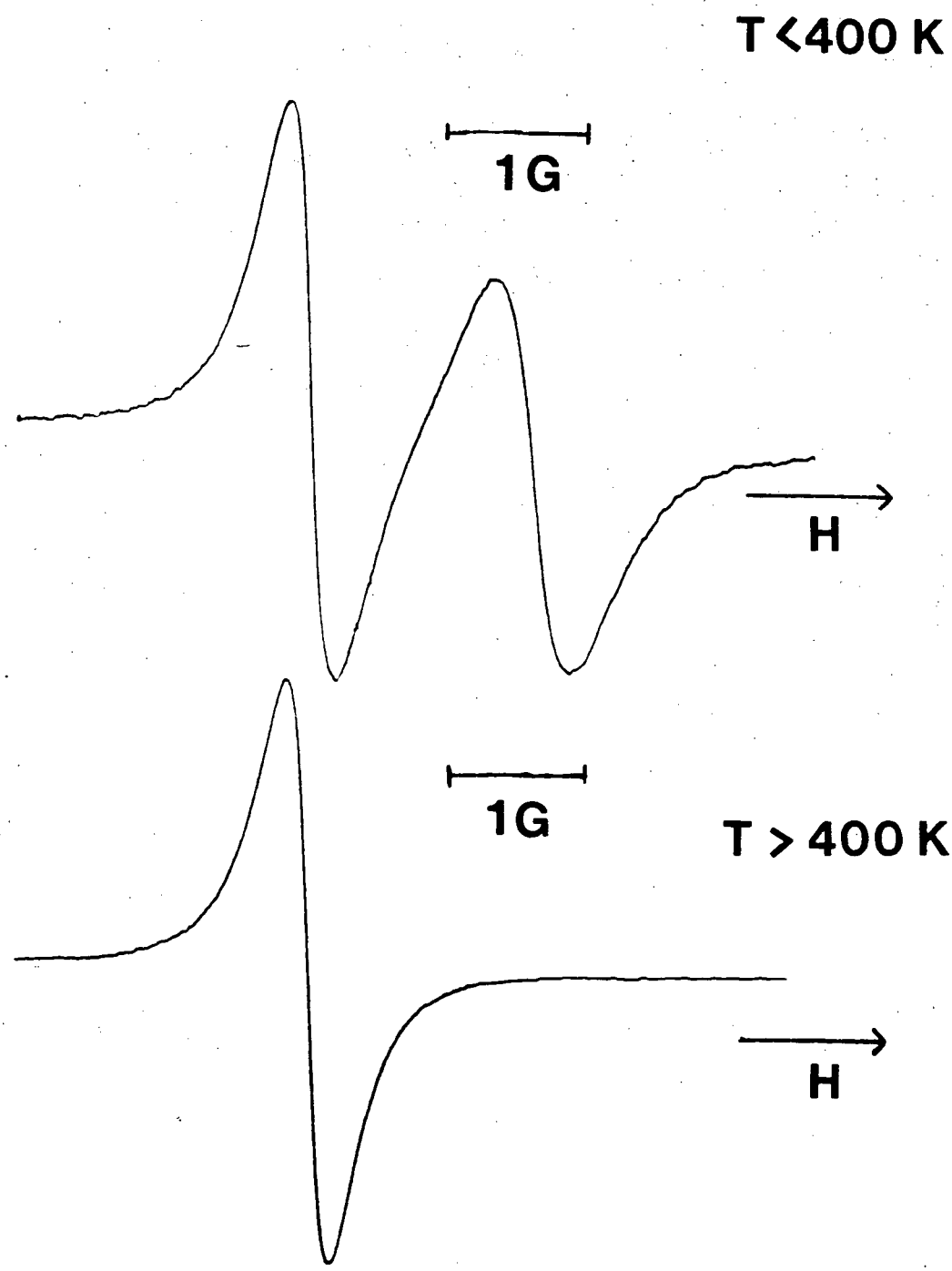

Figure 4.3 Typical ESR Spectra above and below the Phase Transition at 400(3) K.

The spin susceptibilities and peak to peak widths could then be obtained from the Gaussian–Lorentzian functions. Typical ESR spectra below and above the observed phase transition are shown in fig. 4.3.

4.3 CONVOLUTED GAUSSIAN–LORENTZIAN FIT

(a) Fit

The digitized ESR output signal was integrated numerically and then fitted with convoluted Gaussian–Lorentzian functions. The fit was performed by minimizing the sum of square deviations between the data points and the functions.

The susceptibilities of each individual curve were then determined by intergrating the Gaussian–Lorentzian functions obtained from the fit. The corresponding peak to peak half widths were obtained from the derivative of the Gaussian–Lorentzian functions obtained from the fit. This method provided the susceptibilities and peak to peak halfwidths of each individual line in the convoluted ESR spectra below the phase transition. Above the phase transition the susceptibilities and peak to peak halfwidths were determined from a fit of a single convoluted Gaussian–Lorentzian function to the integrated data.

The most significant error in the susceptibility calculation arises from the determination of the baseline;

however in 12% of the data scans significant distortions were found that were not due to integrating a derivative curve with an incorrect baseline. These distortions were due to an asymmetry in the derivative curves. The meaning of the susceptibilities in these cases is suspect, and these scans were not incorporated in the results.

(b) Baseline Determination

The problem of determining the baseline is a significant limitation to the final accuracy of the susceptibilities. The initial estimate of the baseline was determined by averaging the data across the scan.

The integrated data were also found to have distortions that were attributed to problems in baseline removal. There were scans where the tail before the peaks decreased before it increased, this is due to removing too large a baseline, and there were scans where the tail after the peaks increased before it decreased, this is due to removing too small a baseline. These distortions were minimized by making changes to the initial baseline of the order of 0.5% interactively on the UBC computer. The contribution to the error in the susceptibilities from this source could be estimated to be about 10%.

CHAPTER 5 ESR EXPERIMENTAL RESULTS

5.1 ESR g VALUES

At room temperature two lines I and II are found in the spectrum of $DEM(TCNQ)_2$, corresponding to the two stacks B and A. We follow the notation of Schwerdtfeger et al. 1980.

The g values of lines I and II of the ESR spectrum of $DEM(TCNQ)_2$ were determined as a function of temperature between 290 K and 401 K at an angle $\theta = 60°$ (see fig.5.1) The g value was found to be independent of temperature between 290 K and T_c = 400 K. The g values given in table I for $T<T_c$ are the average of the g values measured for $\theta = 60°$ at various temperatures between 290 K and 400(3) K. The g values of both lines below the phase transition and the g value for the single line above the phase transition are summarized in the table below.

TABLE 5.1 ESR g VALUES

Temp.	I	II
$T<T_c$	2.003233(23)	2.002571(17)
$T>T_c$	2.003250(10)	-

The g value below the phase transition was not found to change apart from experimental error. The errors quoted for the g values below T_c are the standard error or the mean of nine measurements at different temperatures below T_c. The errors quoted for the g value above T_c are the standard error of the mean of two results above the phase transition. The above errors do not include any systematic errors from the calibration.

The calibration was performed using a sample of LiF:Li. The g value of Li is 2.002317(2). (Pressley et al 1963, and Gordon et al 1972 p.345 and p.336). The calibration introduces a systematic error of 0.001% to the g value measurements.

These g value data imply that the remaining line above the phase transition is line I.

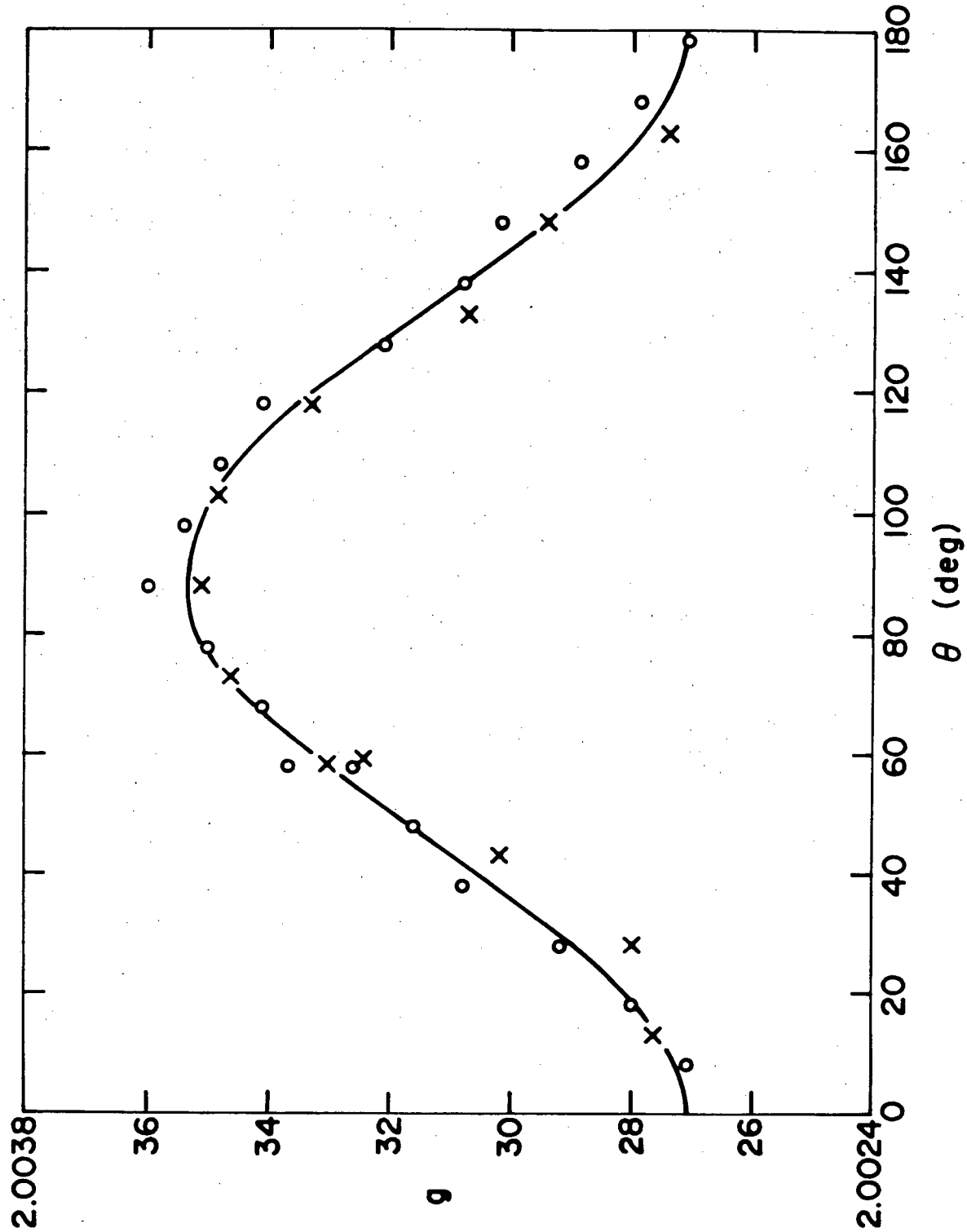

Figure 5.1 Angular dependence of the g value of $DEM(TCNQ)_2$ above the phase transition at 400(3) K ○: crystal #5 ×: repeat run of crystal #5. The solid line is a fit to equation 5.1

5.2 ANGULAR DEPENDENCE OF THE g VALUES

The angular dependence of the g values above the phase transition was measured by rotating the sample in the plane of the static magnetic field. This data is plotted in fig 5.1.

The angular dependence of the g value was fitted to the equation

$$g^2 = g_{\parallel}^2\cos^2\theta + g_{\perp}^2\sin^2\theta \qquad (5.1)$$

The resulting values for $g_{\parallel}$ and $g_{\perp}$ at 401 K together with the values quoted in the literature for lower temperatures (Schwerdtfeger et al 1980) are summarized in table 5.2.

TABLE 5.2 $g_{\parallel}$ AND $g_{\perp}$ FOR DEM(TCNQ)$_2$

Temp. (K)	line I $g_{\parallel}$	line I $g_{\perp}$	line II $g_{\parallel}$	line II $g_{\perp}$
401	2.002730(15)	2.003551(14)	-	-
298	2.00235	2.00325	2.00230	2.00335
77	2.00219	2.00231	2.00223	2.00315
4.2	-	-	2.00270	2.00399
1.14	-	-	2.00147	2.00399

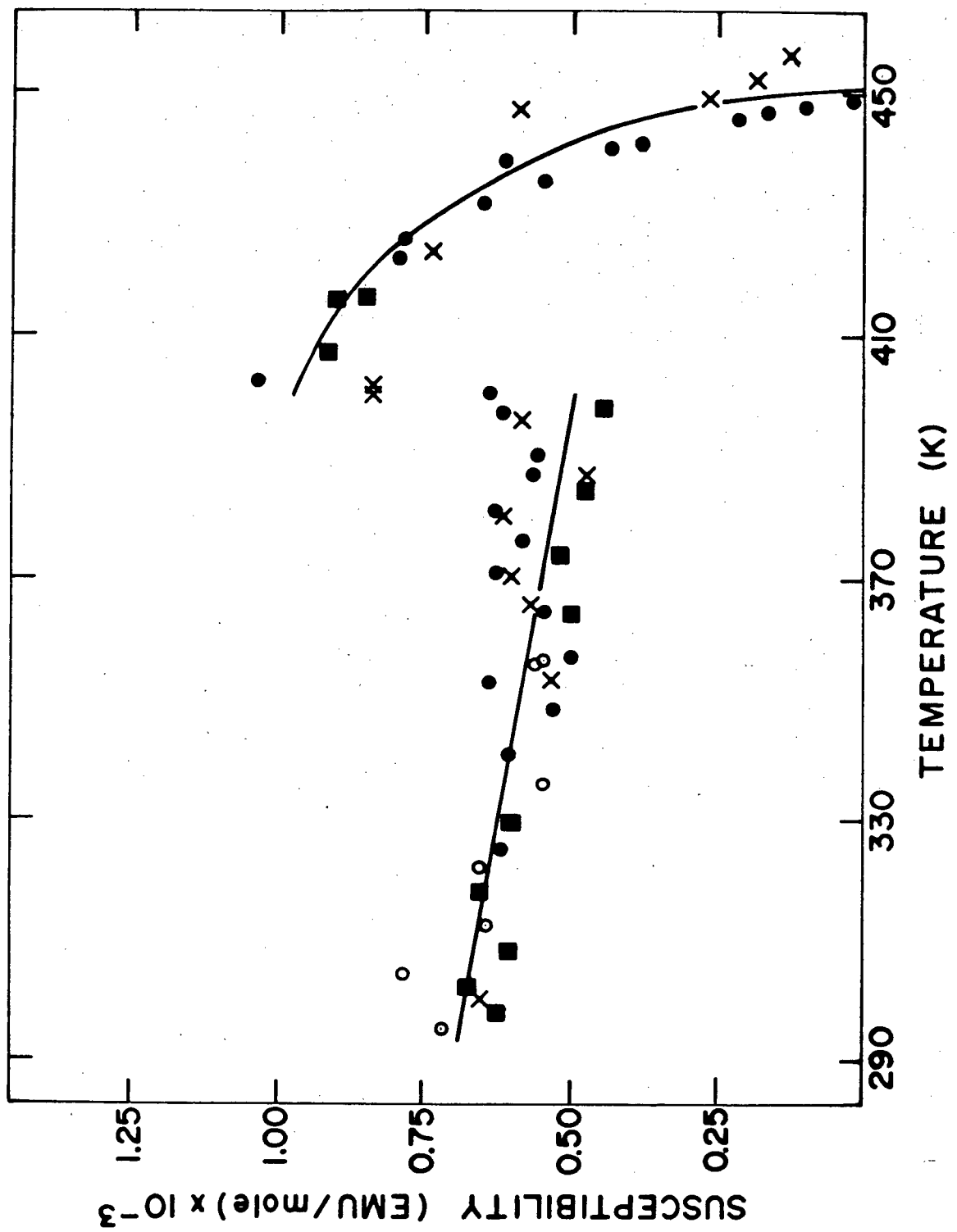

Figure 5.2 Temperature Dependence of the Spin Susceptibility of line I of $DEM(TCNQ)_2$ ■: crystal #4 ○: crystal #5 ×: repeat run of crystal #5 ●: crystal #6 The Solid Curve is Estimated from the Points

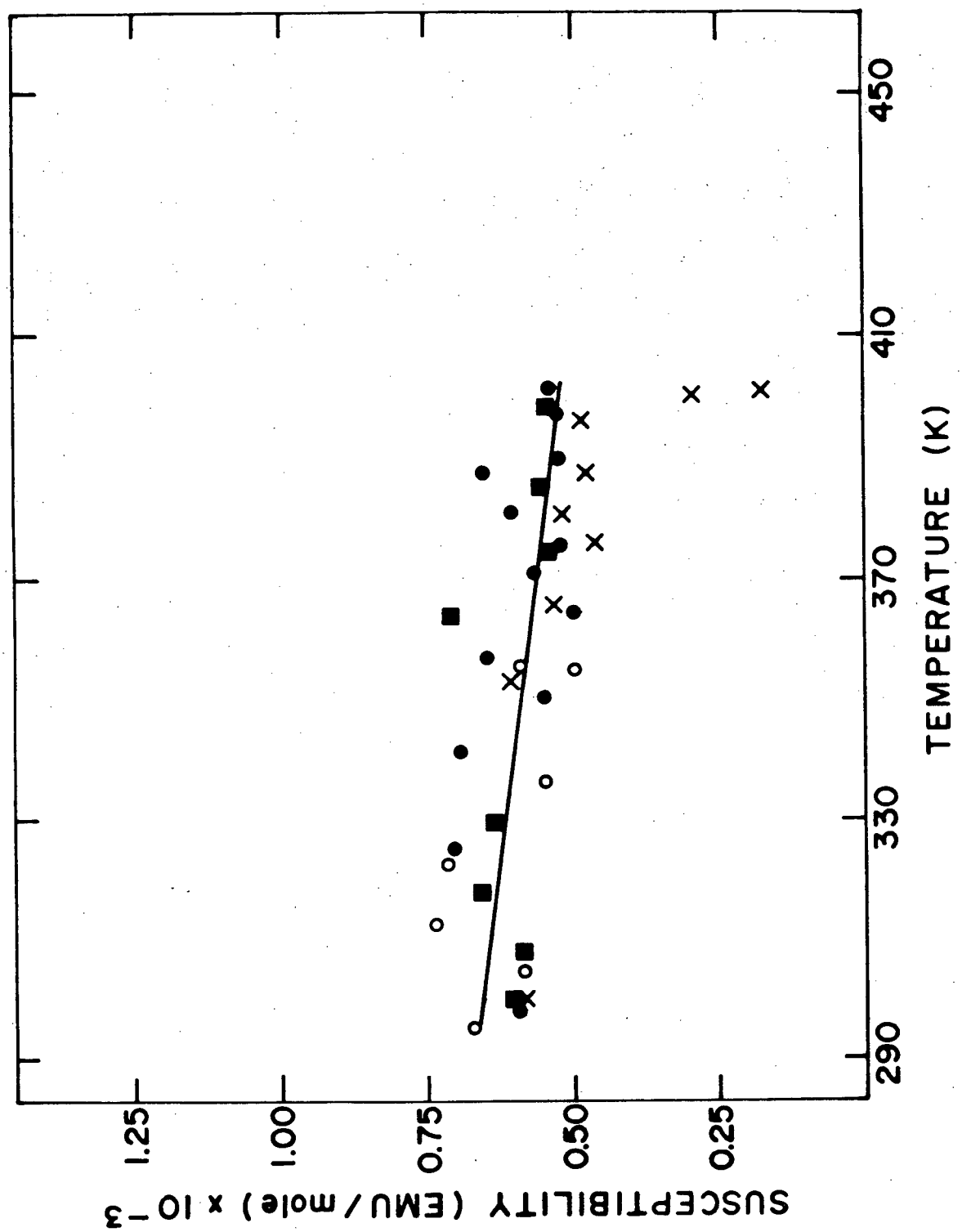

Figure 5.3 Temperature Dependence of the Spin Susceptibility of line II of DEM$(TCNQ)_2$. Symbols are Defined in Fig. 5.2. The Solid Curve is Estimated from the Points.

The quoted experimental error for $g_{||}$ and $g_{\perp}$ is the statistical error from the fit of the data to equation 5.1.

The systematic difference between the values for $g_{||}$ and $g_{\perp}$ at 298 K and at 420 K could be due to a systematic error between the two measurements. This conclusion is reached because the measurements at 298 K were calibrated using DPPH and there was no difference in g value between 298 K and 401 K when both measurements were performed using the same calibration.

5.3 TEMPERATURE DEPENDENCE OF THE SUSCEPTIBILITY

The spin susceptibility of $DEM(TCNQ)_2$ has been measured below 270 K (Schwerdtfeger et al. 1980). The spin susceptibility of lines I and II is shown in figs. 5.2 and 5.3 respectively. The sum of the susceptibilities of lines I and II is plotted in fig. 5.4. From this data we see that the susceptibility of line II goes to zero at 400(3) K. Above 400(3) K only one line is observed, indicating a phase transition at 400(3) K. The spin susceptibility of line I increases at 400(3) K and the combined susceptibility curve is continuous across the phase transition. We have seen that the g value of line I before the phase transition is the same as the g value of the single line above the phase transition (see section 5.1). This together with the susceptibility data indicates that there is a transfer of spin from stack A to stack B at 400(3) K. There is at present no physical explanation for this transfer of spin.

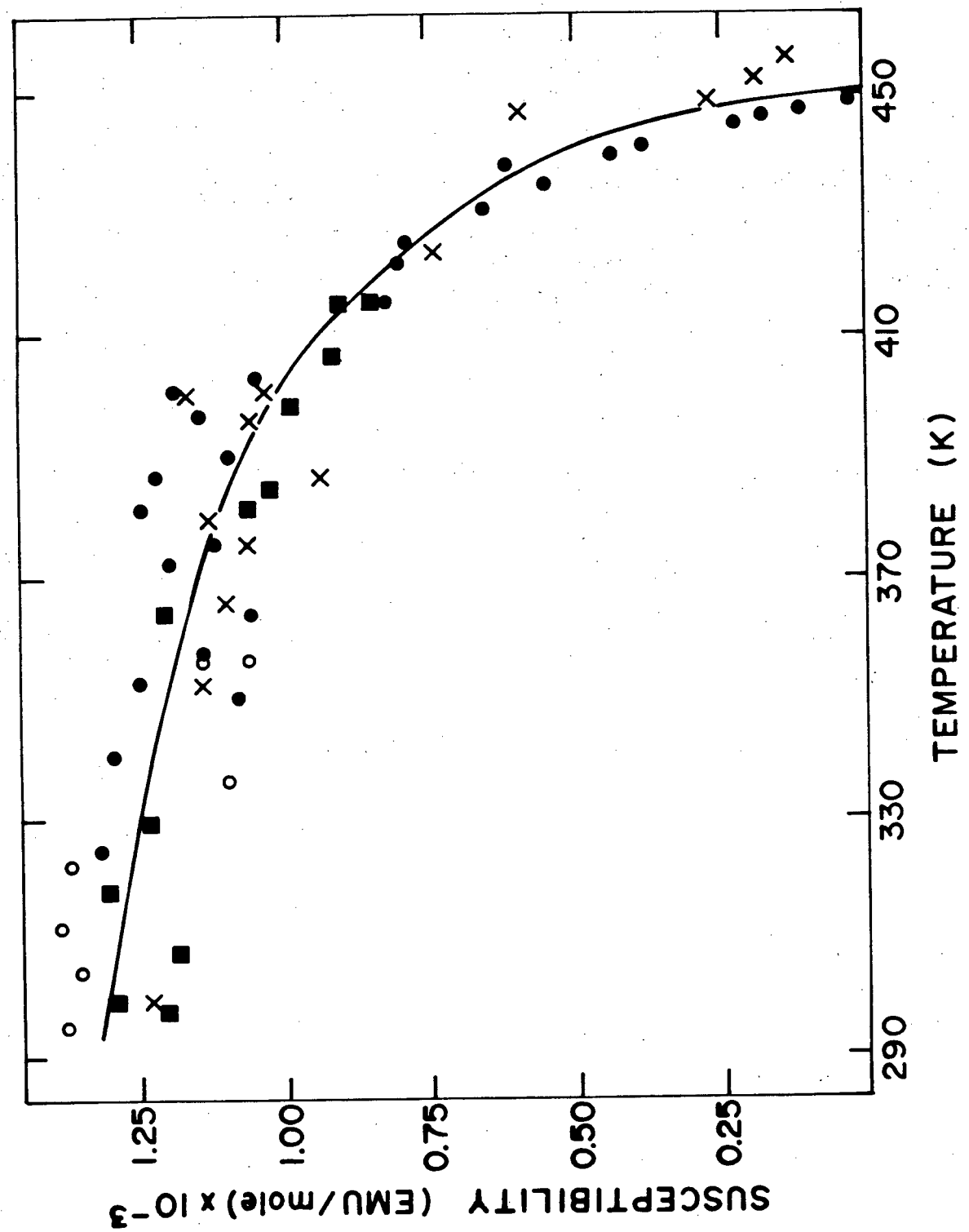

Figure 5.4 Temperature Dependence of the Sum of the Spin Susceptibilities of lines I and II of $DEM(TCNQ)_2$. Symbols are Defined in Fig. 5.2 The Solid Curve is Estimated from the Points

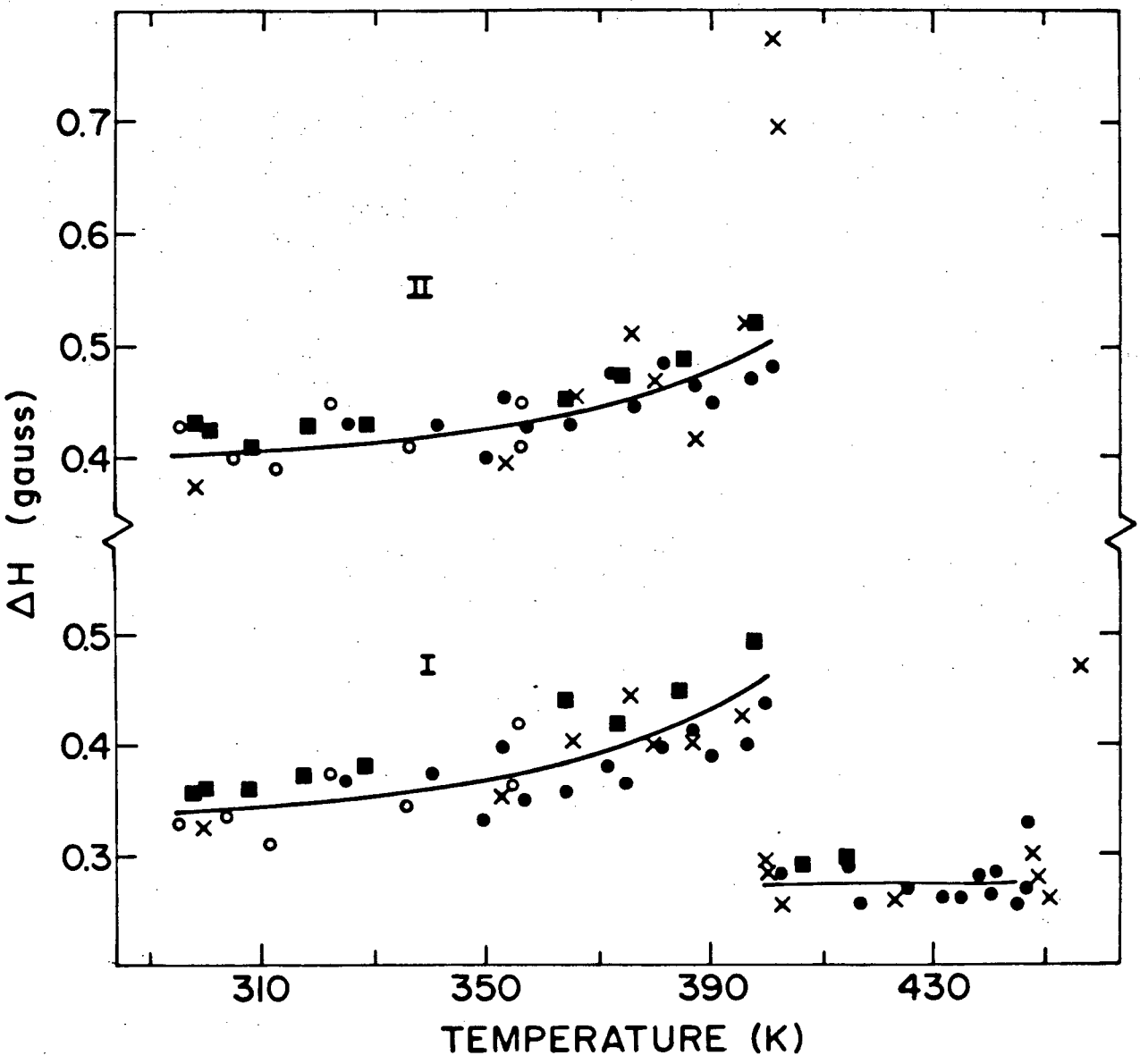

Figure 5.5 Temperature Dependence of the Peak to Peak Halfwidth of Lines I and II of $DEM(TCNQ)_2$. Symbols are Defined in Fig. 5.2

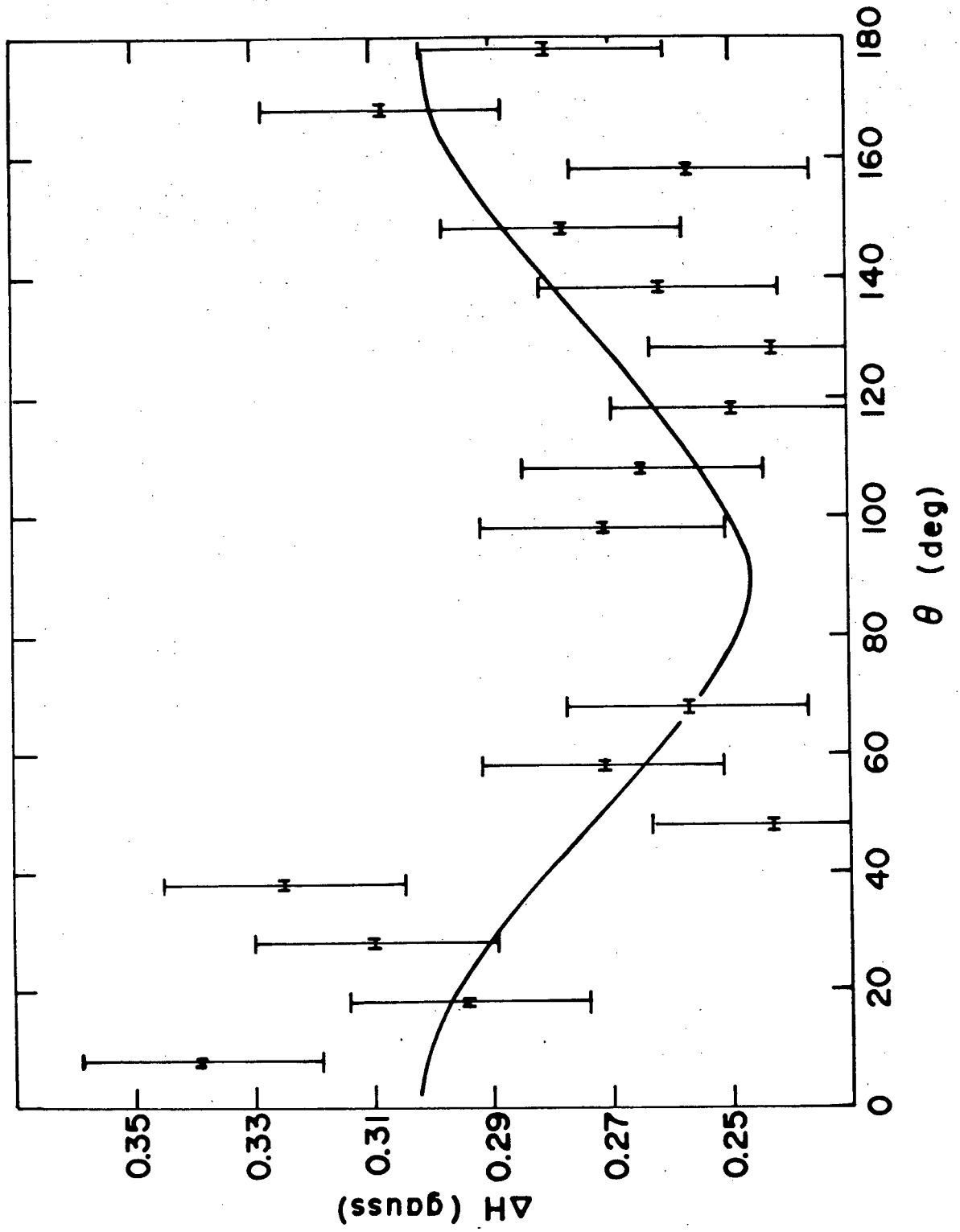

Figure 5.6 Angular Dependence of the Peak to Peak Halfwidth of line I of $DEM(TCNQ)_2$ above the phase transition at 400(3) K. The Solid Line is a Fit to $H^2 = H_{\parallel}^2\cos^2\theta + H_{\perp}^2\sin^2\theta$.

The phase transition at 400(3) K was found to be reversible. Sample #5 was taken past the phase transition to 401 K and then cooled back to room temperature. The repeat measurements of sample #5 were no different in the susceptibility or the g value.

Between 415 K and 453(6) K the combined susceptibility decreases sharply to zero and does not follow the high temperature tail of the Curie–Wiess law. This decrease in the susceptibility, however, is irreversible. A repeat measurement after the sample has been cooled to room temperature produces no ESR signal

The scatter in the data of the susceptibility as a function of temperature, arises from the error in the determination of the Gaussian–Lorentzian fitting functions. These errors arise from the determination of the baseline.

5.4 TEMPERATURE DEPENDENCE OF THE PEAK TO PEAK WIDTHS OF THE ESR LINES

The peak to peak width of the ESR lines was measured as a function of temperature between 290 K and 453(6) K. The data are plotted in fig 5.5. The peak to peak widths were calculated by a double numerical intergration of each Gaussian–Lorentzian function obtained from the fit.

The data show a broadening of both lines with increasing temperature as the phase transition temperature, 400(3) K, is

approached from below. The phase transition at 400(3) K is accompanied by a discontinous drop in the peak to peak halfwidth of line I, and the disappearance of line II.

The peak to peak halfwidth as a function of angle for stack B above the phase transition is plotted in fig 5.6. The halfwidth in this case was measured directly from the ESR scans. The angular dependence of the halfwidth reaches a minimum for the same θ where the angular dependence of the g values exhibits a maximum (see fig 5.1). This result is similar to that reported by Schwerdtfeger et al (1980) for stack A at 77 K

The scatter in the peak to peak halfwidth vs temperature curve arises from the determination of the Gaussian–Lorentzian fitting function. The most significant contribution to these errors is the determination of the baseline (see section 4.3). The estimated errors in the peak to peak halfwidth as a function of angle are are estimated from the ESR data scans.

CHAPTER 6 DISSCUSION OF THE RESULTS

6.1 PHASE TRANSITIONS IN DEM(TCNQ)$_2$

The ESR measurements show a reversible phase transition at 400(3) K, where the susceptibility of line II goes into line I. At this temperature there is no indication of a phase transition in the microwave conductivity or in the total spin susceptibility.

This phase transition is explained by a transfer of spin density from stack B to stack A. The fact that the conductivity and spin susceptibility are continuous over this phase transition and that the spin susceptibility equals the value of the spin susceptibility immediately below the phase transition at 400(3) K implies that the contribution to the conductivity and to the susceptibility from stack A and stack B are equal. Non-reversible effects in the susceptibility are observed above 415 K while below this temperature the crystal behaves in a reversible manner. These non-reversible effects could possibly be due to the onset of the decomposition of the sample.

At a temperature of 442(6) K a non-reversible phase transition in the microwave conductivity is observed. Between 420 K and 453(6) K the spin susceptibility decreases

irreversibly to zero. This indicates that the decrease of the spin susceptibility to zero and the discontinuity in the conductivity are different manifestations of the same phase transition.

The decrease of the conductivity between 460 K and 480 K was found to be due to a decomposition of the sample. On the other hand temperature dependent Guinier photographs of $DEM(TCNQ)_2$ showed two reversible phase transitions at 415 K and 483 K. (Morrsink et al 1980).

We postulate that the phase transition at 442(6) K to 453(6) K and the Guinier measurement at 483 K are related. Similarly we postulate that the reversible phase transition at 400(3) K is related to the phase transition at 415 K obtained by the Guinier measurement. A possible explanation is that these two phase transitions occur over a range of temperatures, with the electronic effects occurring before the structural effects. These differences in the phase transition temperatures can also be explained by the different rates at which the sample was heated in the various experiments, the slowest rate being the conductivity measurement with the lowest phase transition temperature, then the ESR measurements and finally the Guinier measurements with the fastest rate of heating and the highest phase transition temperature. Although this requires further investigation, a similar pattern is seen in the other compounds as noted below.

6.2 COMPARISON OF $DEM(TCNQ)_2$ TO $HEM(TCNQ)_2$ AND $MEM(TCNQ)_2$

The ESR of $HEM(TCNQ)_2$ exhibits a phase transition at 425 K with a decrease to zero of the spin susceptibility and a differential scanning calorimeter (DSC) measurement of $HEM(TCNQ)_2$ exhibits a phase transition at 450 K. (Huizinga 1980 p.108).Temperature dependent Guinier photographs of $HEM(TCNQ)_2$ exhibit a phase transition at 456 K (van Bodegom, 1979, p.73). This corresponds to the $2k_F$ phase transition in $HEM(TCNQ)_2$ (Huizinga 1980 p.108). These differences in phase transition temperatures are very similar to those reported for $DEM(TCNQ)_2$ above.

In $MEM(TCNQ)_2$ we find both the $2k_F$ and the $4k_F$ instabilities. The $2k_F$ instability has been attributed to the Spin–Peierls phase transition at 18 K while the $4k_F$ phase transition has been attributed to the semiconductor–metal phase transition at 335 K (Huizinga 1980).

The question of how the phase transitions in $MEM(TCNQ)_2$ and $HEM(TCNQ)_2$ relate to the phase transitions B of $DEM(TCNQ)_2$ remains to be answered. The Spin–Peierls phase transition in $MEM(TCNQ)_2$ at 18 K is close to the Spin–Peierls phase transition at 23 K in stack B of $DEM(TCNQ)_2$. The nature of the two phase transitions above room temperature in $DEM(TCNQ)_2$ should indicate which phase transition corresponds to the $4k_F$ instability in stack B of $DEM(TCNQ)_2$.

The phase transition at 400(3) K is related to stack A. There is a transfer of spin density from stack A to stack B, but there is no effect on the total bulk susceptibility or the

conductivity to within the scatter in the data. The radical effects on the susceptibility and the conductivity are observed at 453(6) K and 442(6) K respectively, indicating that this phase transition may correspond to the $4k_F$ instability. This however is not clear because of the decomposition of the sample.

The latter phase transition in $DEM(TCNQ)_2$ is however different from the semiconductor–metal phase transition in $MEM(TCNQ)_2$ in that no metallic conductivity is observed above this phase transition. This however can be explained because the phase transition temperature in $DEM(TCNQ)_2$ is higher than in $MEM(TCNQ)_2$, namely because of the probable decomposition of the $DEM(TCNQ)_2$ sample. There are also some similarities between the highest phase transition in $DEM(TCNQ)_2$ and the phase transition at 425 to 450 K in $HEM(TCNQ)_2$ in that in both phase transitions the susceptibility decreases to zero and there are temperature discrepancies of 30 K and 31 K between the decrease of the susceptibility to zero and the Guinier measurements respectively. The cause of the temperature discrepancy in both cases is probably the speed at which both kinds of measurements were made or a difference in the temperature between the electronic and the structural effects. The proximity in the temperatures of these two phase transitions could also account for some of the similarities.

CHAPTER 7 CONCLUSIONS AND FURTHER POSSIBLE EXPERIMENTS

7.1 CONCLUSIONS

The ESR and microwave conductivity of DEM$(TCNQ)_2$ above room temperature showed two phase transitions. Firstly a reversible phase transition at 400(3) K where there was a transfer of spin density from stack A to stack B. The angular dependence of the g value of the single line above this phase transition was identical to that of line I. This phase transition was not observed in a measurement of the total spin susceptibility nor in a measurement of the microwave conductivity. The second phase transition was observed between 442(6) K and 453(6) K. This is a non-reversible phase transition that was manifested by a discontinuity in the microwave conductivity and the decrease to zero of the total spin susceptibility. This phase transition is possibly due to the 4k instability in stack B of DEM$(TCNQ)_2$. The phase transition temperatures determined by the ESR and microwave conductivity methods were lower than the Guinier photograph results for both phase transitions.

7.2 FURTHER DIRECTIONS

There are many possibilities for further research on related TCNQ compounds; however we will only consider further experiments in $DEM(TCNQ)_2$ that are suggested by this work:

(a) A study of the dependence of the phase transition temperatures on the rate of heating of the crystal. The times involved would be from 6-hours to 1-2 days for heating the sample from room temperature to about 480 K. This would clarify the discrepancy in the phase transition temperatures between the ESR and microwave conductivity measurements and the Guinier photograph measurements.

(b) The real part of the dielectric constant can be measured as a function of temperature past these phase transitions. This experiment is contingent on obtaining thin long crystals of $DEM(TCNQ)_2$ which are very difficult to grow.

BIBLIOGRAPHY

van Bodegom, B., and van de Boer, J. L., Acta. Cryst B37, 1195 (1981)

Bosh, A., and van Bodegom, B., Acta. Cryst. B33, 3013 (1977)

Buranov, L. I., and Shchegolev, I. F., Instruments and Experimental Techniques 14, 528 (1971)

Gordon, A. J., and Ford, R. A., The Chemical Companion: A Handbook of Practical Data Techniques and References (John Willey and Sons: New York, 1972)

von Hippel, A., Tables of Dielectric Materials (Laboratory for Insulation Research, Massachusetts Institute of Technology)

Huizinga, S., PhD Thesis, University of Groningen (1980)

Huizinga, S., Kommandeur, J., Sawatzky, G. A., and Thole, B. T., Phys Rev B19, 4723 (1979)

Kuindersma, P. I., Sawatzky, G. A., and Kommandeur, J., J. Physics C (Solid State) 8, 3005 (1975).

Morrow, M., Hardy, W. N., Carolan, J. F., Berlinsky, A. J., Weiler, L., Gujral, V. K., Janossy, A., Holczer, K., Mihlay, G., Grüner, G., Huizinga, S., Verwey, A., and Sawatzky, G. A., Can. J. of Phys. 58 334 (1980)

Morrsink, H., and van Bodegom, B., Acta Cryst. 37, 107 (1981)

Osborn, J. A., Phys. Rev. 60 351 (1945)

Pressley, R. J., and Berk, H. L., Bull. Am. Phys. Soc. 8, 345 (1963)

Sawatzky, G. A., Huizinga, S., and Kommandeur, J., Proceedings of the International Conference on Quasi-one-dimensional Conductors, September 1978 Dubrobnik Yugoslavia, Lecture Notes in Physics p. 34, (Berlin: Springer Verlag, 1978)

Schwerdtfeger, C. F., Oostra, S., and Sawatzky, G. A., Phys Rev (In print 1981)

Schwerdtfeger, C. F., Wagner, H. J., and Sawatzky, G. A., Solid State Comm. 35, 7 (1980)

Waldron, R. A., Theory of Guided Electromagnetic Waves (London: van Nostrand Reinhold Company, 1970)

Waldron, R. A., The Theory of Waveguides and Cavities (New York: Gordon and Breach Science Publishers, 1969)